

Electronic Supplementary Information (ESI)

Content

1. Synthesis of MCPs
2. PXRD patterns of UMCM-10, -11, -12
3. Single crystal X-Ray diffraction for UMCM-10, -12
4. ¹H NMR spectroscopic data of UMCM-10, -11, -12
5. TGA traces of activated UMCM-10, -11, -12
6. Gas sorption measurements for UMCM-4, -10, -11, -12
7. PXRD patterns of UMCM-4, -10, -12 at elevated temperatures and air
8. Microscopic images after dye diffusion experiments
9. Linear dichroism experiment for UMCM-4

1. Synthesis of MCPs:

2,2',6,6'-tetramethylbiphenyl-4,4'-dicarboxylic acid (H₂-TMBPDC),¹ 4,4'-(ethyne-1,2-diyl)dibenzoic acid (H₂-EDDB),² 2',3',5',6'-terramethylterphenyl-4,4''-dicarboxylic acid (H₂-TMTPDC)³ were synthesized following the reported methods.

A) Preparation of Zn₄O(TPA)(BDC)_{1/2}(TMBPDC): UMCM-10.

H₂-BDC (5.48 mg, 0.0330 mmol), H₂-TMBPDC (19.7 mg, 0.0667 mmol), H₃-TPA (12.5 mg, 0.0330 mmol) and Zn(NO₃)₂ · 6H₂O (119 mg, 0.400 mmol) were dissolved in 5.0 mL of *N,N*-diethylformamide. The mixture was sonicated for 15 min and the solution was clarified by filtration through a glass wool plug. The reaction mixture was heated to 85 °C. After 2 days, crystals of a single phase were obtained. After cooling to room temperature, the product was isolated by decanting the mother liquor and washing with fresh DMF (3 × 15 mL). The yield of the reaction determined from the weight of the solvent-free material (17.3 mg) is 52.4% based on H₃-TPA.

B) Preparation of Zn₄O(TPA)(BDC)_{1/2}(EDDB): UMCM-11.

H₂-BDC (5.48 mg, 0.0330 mmol), H₂-EDDB (17.6 mg, 0.0667 mmol), H₃-TPA (12.5 mg, 0.0330 mmol) and Zn(NO₃)₂ · 6H₂O (119 mg, 0.400 mmol) were dissolved in 5.0 mL of 1:1 (v/v) *N,N*-diethylformamide and *N*-methylpyrrolidinone. The mixture was sonicated for 15 min and the solution was clarified by filtration through a glass wool plug. The reaction mixture was heated to 85 °C. After 5 days, crystals of a single phase were obtained. After cooling to room temperature, the product was isolated by decanting the mother liquor and washing with fresh DMF (3 × 15 mL). The yield of the reaction determined from the weight of the solvent-free material (17.0 mg) is 51.6% based on H₃-TPA.

C) Preparation of Zn₄O(TPA)(BDC)_{1/2}(TMTPDC): UMCM-12.

H₂-BDC (6.72 mg, 0.0405 mmol), H₂-TMTPDC (14.96 mg, 0.040 mmol), H₃-TPA (7.57 mg, 0.0201 mmol) and Zn(NO₃)₂ · 6H₂O (89.2 mg, 0.300 mmol) were dissolved in 5.1 mL of *N,N*-diethylformamide. The mixture was sonicated for 40 min and the solution was clarified by filtration through a glass wool plug. The reaction mixture was heated to 85 °C. After 12 hours, crystals of a single phase were obtained. After cooling to room temperature, the product was isolated by decanting the mother liquor and washing with fresh DMF (3 × 15 mL). The yield of the reaction determined from the weight of the solvent-free material (10.0 mg) is 50.1% based on H₃-TPA.

2. PXRD patterns of UMCM-10, -11, -12

Samples for powder X-ray diffraction were soaked in mineral oil before collection of data. Data were collected on Rigaku R-Axis Spider diffractometer with an image plate detector and $\text{CuK}\alpha$ radiation operating in transmission mode. The powder samples were rotated on the goniometer in φ and oscillated in ω to minimize preferred orientation. (Figures S1, S2, and S3)

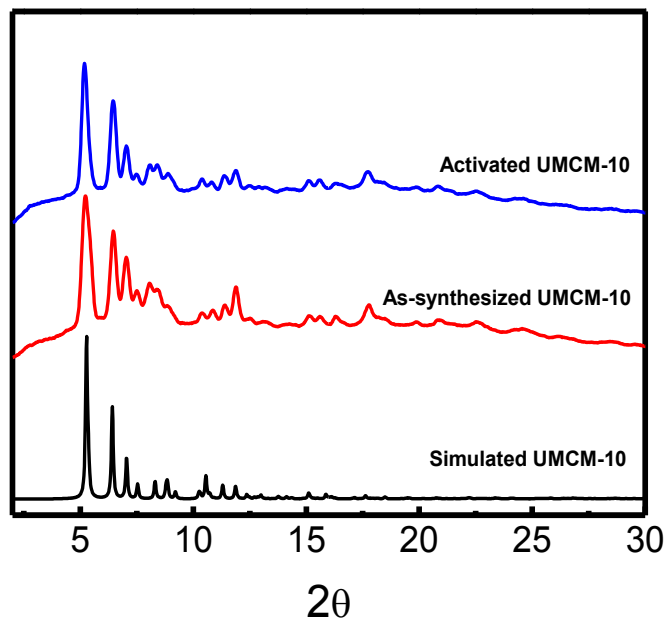


Figure S1. Powder XRD patterns of UMCM-10 (black: simulated, red: as synthesized, blue: activated).

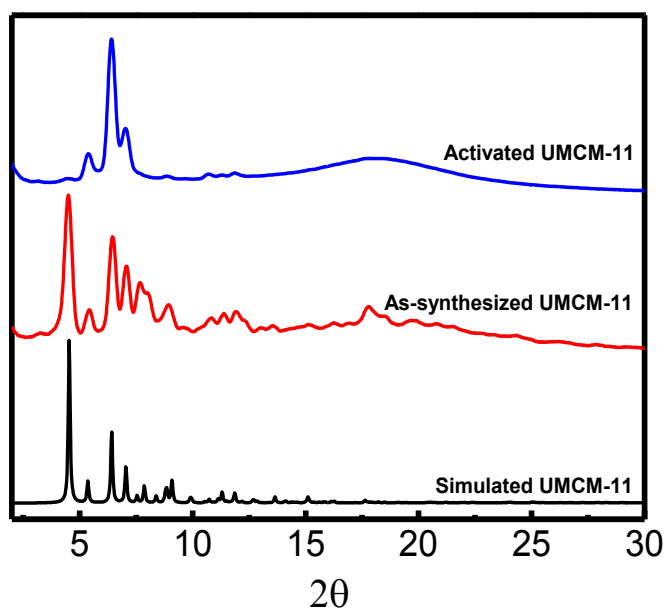


Figure S2. Powder XRD patterns of UMCM-11 (black: simulated, red: as synthesized, blue: activated).

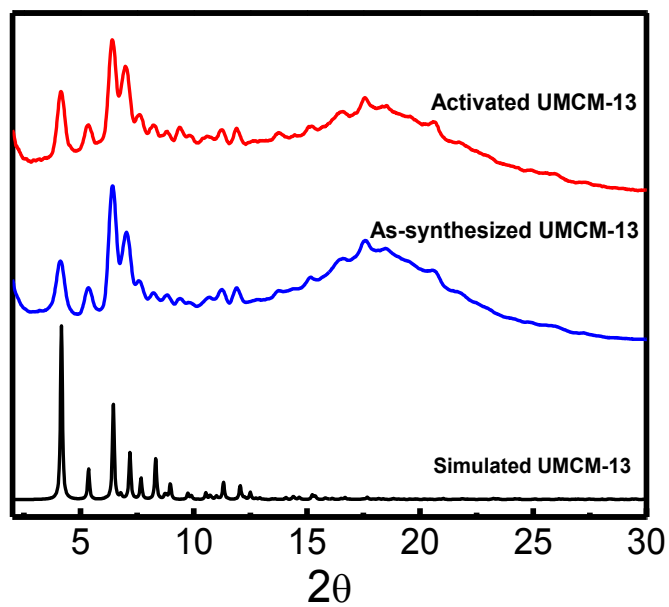


Figure S3. Powder XRD patterns of UMCM-12 (black: simulated, blue: as synthesized, red: activated).

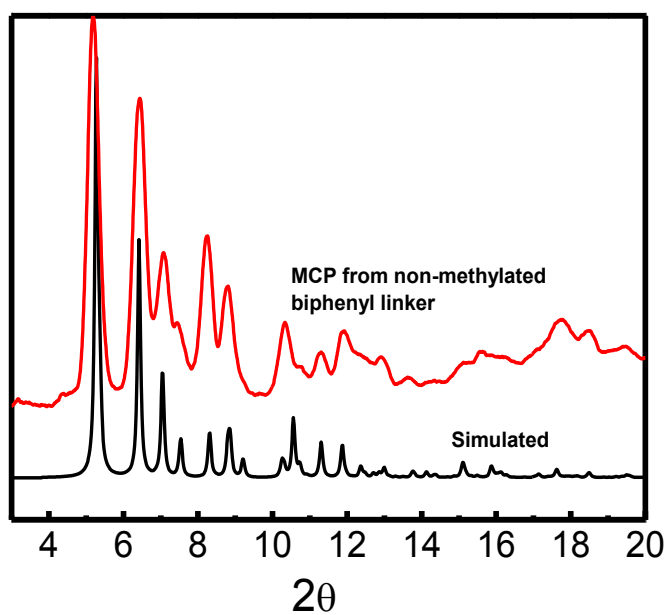


Figure S4. Powder XRD patterns of MCP synthesized using terphenyl pillar linker (black: simulated, red: experimental).

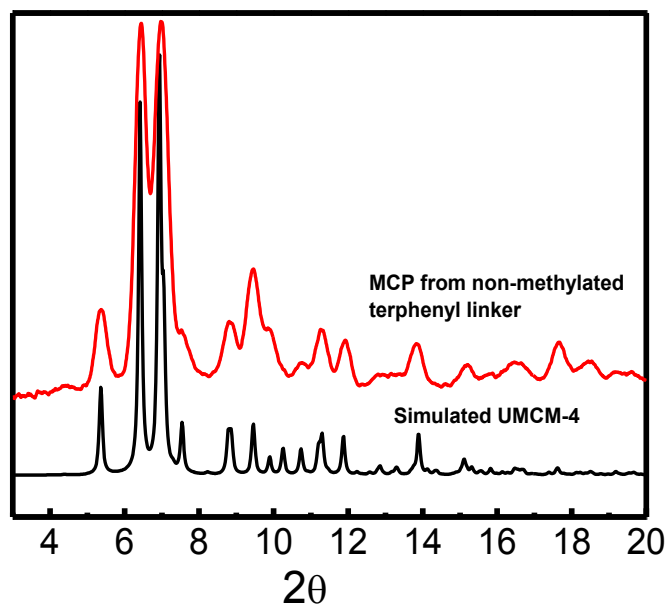


Figure S5. Powder XRD patterns of MCP synthesized using terphenyl pillar linker (black: simulated UMCM-4, red: experimental).

3. Single crystal X-Ray diffraction for UMCM-10 and -12

Crystals of UMCM-10 [$\text{Zn}_4\text{O}(\text{TPA})(\text{TMBPDC})(\text{BDC})_{0.5}$] exchanged in CH_2Cl_2 were coated in Paratone N oil. A clear block of a crystal ($0.18 \times 0.12 \times 0.10 \text{ mm}^3$) was mounted on a MitiGen MicroMount tip. X-ray diffraction data were collected on a Rigaku R-Axis Spider diffractometer (460 mm \times 256 mm curved imaging plate detector, crystal-to-detector distance was 127.40 mm, graphite monochromated Cu $K\alpha$ radiation at 2 kW power) at 233 K. A total of 401 oscillation images were collected using widths of 1.5° in ω . The exposure time was 8 minutes for all images. Data were collected using the d*TREK package in the CrystalClear software suite (v. 2.0, Rigaku 2009) to obtain overlapping ϕ and ω scans. Using the FS_PROCESS package in CrystalClear, the raw intensity data were then reduced to F^2 values with corrections for Lorentz, and polarization effects. Decay of the crystal during data collection was negligible. An empirical absorption correction was applied as implemented by FS_PROCESS. The structure was solved by direct methods and refined against all data using the CrystalStructure (v. 4.0) software package in the monoclinic space group $P2_1/c$ (#14) $Z = 4$ using SHELXL-97 in the crystal structure (v. 4.0) software package.⁴ Hydrogen atoms were placed at calculated positions (C-H = 0.93 Å) using a riding model with isotropic thermal parameters 1.2 times that of the attached carbon atom. Thermal parameters for all non-hydrogen atoms were refined anisotropically.

Crystals of UMCM-12 [$\text{Zn}_4\text{O}(\text{TPA})(\text{TMTTPDC})(\text{BDC})_{0.5}$] exchanged in CH_2Cl_2 were coated in Paratone N oil. A clear block of a crystal ($0.18 \times 0.18 \times 0.06 \text{ mm}^3$) was mounted on a cryoloop. X-ray diffraction data were collected on a Rigaku AFC10K Saturn 944+ CCD-based X-ray diffractometer equipped with a low temperature device and Micromax-007HF Cu-target micro-focus rotating anode ($\lambda = 1.54187 \text{ \AA}$) operated at 1.2 kW power (crystal-to-detector distance was 42.00 mm) at 95K. A total of 2068 images were collected with an oscillation width of 1.0° in ω . The exposure time was 10 sec. for the low angle images, 45 sec. for high angle. Analysis of the data showed negligible decay during data collection; the data were processed with CrystalClear 2.0 and corrected for absorption. The structure was solved and refined with the Bruker SHELXTL (version 2008/4) software package, using the space group Pnma with $Z = 4$ for the formula $\text{C}_{98}\text{H}_{68}\text{N}_2\text{O}_{26}\text{Zn}_8$. All non-hydrogen atoms were refined anisotropically with the hydrogen atoms placed in idealized positions. Full matrix least-squares refinement based on F^2 converged at $R1 = 0.0651$ and $wR2 = 0.1473$ [based on $I > 2\sigma(I)$], $R1 = 0.0966$ and $wR2 = 0.1525$ for all data. The SQUEEZE⁵ subroutine of the PLATON program suite was used to address the disordered solvent/oil in the large cavity present in the structure.

Table S1. Crystal data and structure refinement for UMCM-10 and -12

Compound	UMCM-10	UMCM-12
Empirical formula	C ₄₃ H ₃₀ NO ₁₃ Zn ₄	C ₉₈ H ₆₈ N ₂ O ₂₆ Zn ₈
Formula Weight	1030.23	2212.50
Temperature of run	233K	95K
Crystal dimensions	0.18 × 0.12 × 0.10 mm ³	0.18 × 0.18 × 0.06 mm ³
Wavelength	1.54187 Å	1.54187 Å
Crystal system	Monoclinic	Orthorhombic
Space group	<i>P</i> 2 ₁ / <i>c</i>	<i>Pnma</i>
Unit cell parameters	a = 17.1259(4) Å b = 32.5986(8) Å c = 25.1806(18) Å 13866.2(11) Å ³ α = 90° β = 99.471(7)° γ = 90°	a = 24.8949(5) Å b = 42.564(3) Å c = 32.7857(6) Å 34741(3) Å ³ α = 90° β = 90° γ = 90°
Z	4	4
Density (calculated)	0.493 g/cm ³	0.423 g/cm ³
Absorption coefficient	0.957 mm ⁻¹	0.776 mm ⁻¹
F(000)	2076	4472
Theta range for data collection	6.64 to 66.53	2.08 to 65.08
Index ranges	-20 ≤ h ≤ 19, -37 ≤ k ≤ 37, -23 ≤ l ≤ 29	-29 ≤ h ≤ 29, -50 ≤ k ≤ 50, -38 ≤ l ≤ 38
Reflections collected	108598	473511
Independent reflections	24085 [R(int) = 0.0727]	30035 [R(int) = 0.2638]
Completeness to highest theta	98.4 %	99.9 %
Absorption correction	multi-scan	Semi-empirical from equivalents
Max. and min. transmission	1.000 and 0.724	0.9549 and 0.8729
Refinement method	Full-matrix least-squares on F ²	Full-matrix least-squares on F ²
Data/ Restraints/ parameter	24085 / 0 / 550	30035 / 381 / 604
Goodness of fit on F ²	1.197	1.033
Final R indices [I > 2σ(I)] ^{a,b}	R1 = 0.109, wR2 = 0.3315	R1 = 0.0651, wR2 = 0.1473
R indices (all data) ^{a,b}	R1 = 0.1594, wR2 = 0.3829	R1 = 0.0966, wR2 = 0.1525

$wR2 = \frac{|\sum w(|F_o|^2 - |F_c|^2)|}{\sum w(F_o)^2}^{1/2}$, $w = 1 / [\sigma^2(F_o^2) + (mP)^2 + nP]$ and $P = [\max(F_o^2, 0) + 2F_c^2] / 3$ (m and n are constants); $\sigma = [\sum (w(F_o^2 - F_c^2)^2) / (n - p)]^{1/2}$ b) $R1 = \frac{\sum ||F_o| - |F_c||}{\sum |F_o|}$

4. ^1H NMR spectroscopic data for UMCM-10, -11, -12

Solvent free materials were digested in 20% DCl in D_2O diluted with d^6 -DMSO solution before performing NMR spectroscopic experiments. (Figures S4, S5, and S6)

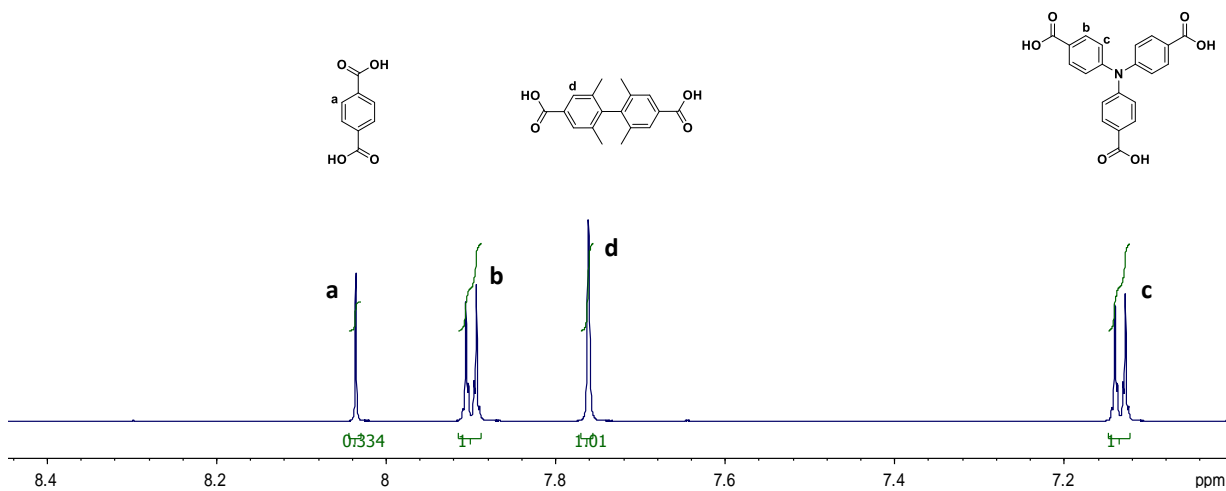


Figure S6. ^1H NMR spectrum of activated UMCM-10 digested in 20% DCl in D_2O diluted with d^6 -DMSO.

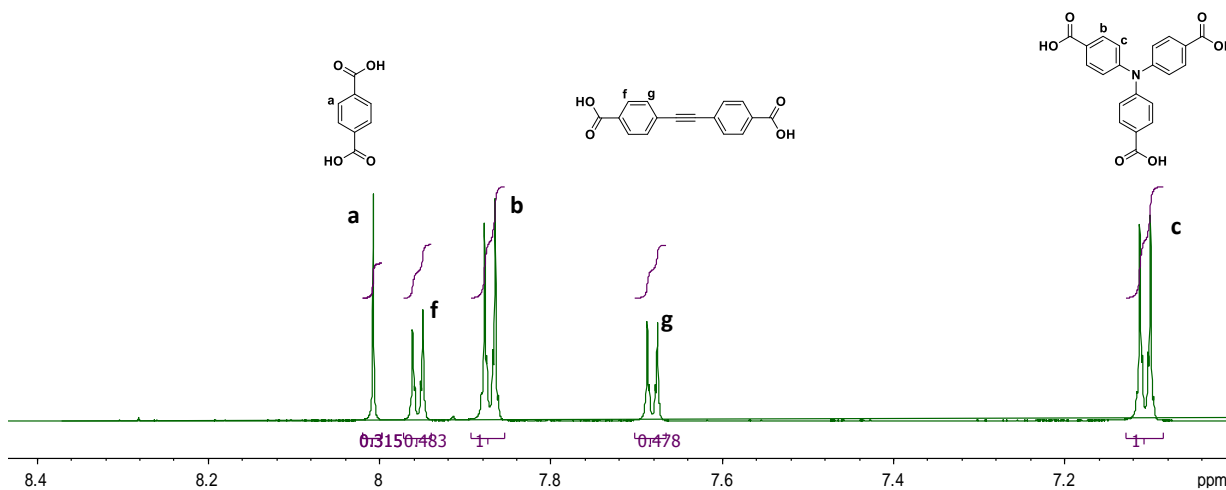


Figure S7. ^1H NMR spectrum of activated UMCM-11 digested in 20% DCl in D_2O diluted with d^6 -DMSO.

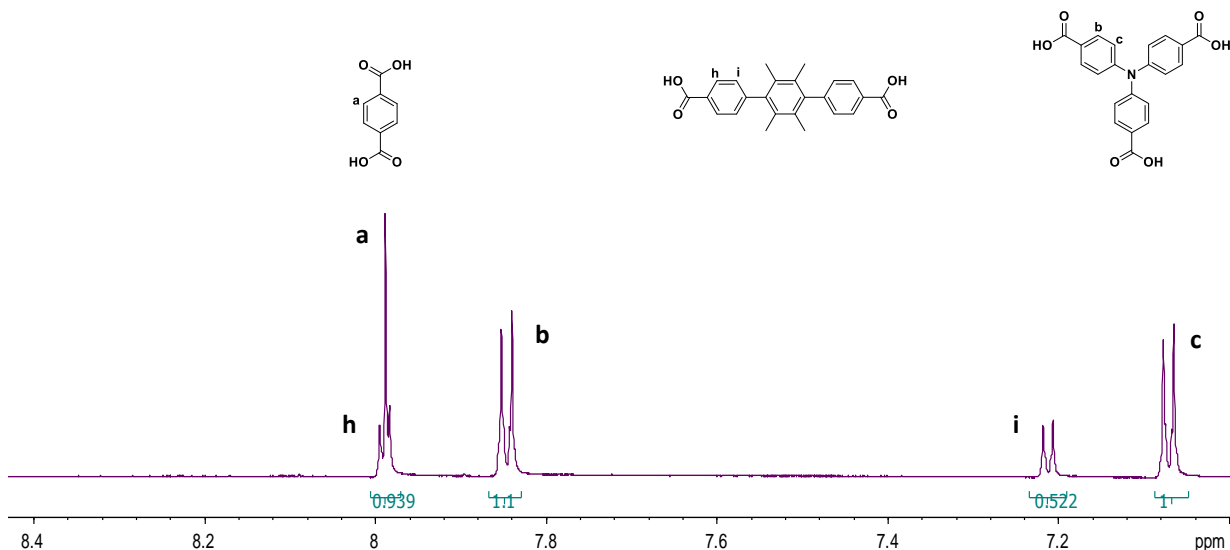


Figure S8. ^1H NMR spectrum of activated UMCM-12 digested in 20% DCl in D_2O diluted with d^6 -DMSO.

5. TGA traces of UMCM-10, -11, -12

Thermogravimetric analyses were performed on a TA Instruments Q50. Samples were evacuated prior to analysis. The temperature was ramped from 25 $^\circ\text{C}$ to 600 $^\circ\text{C}$ with a rate of 2 $^\circ\text{C}/\text{min}$ under a flow of N_2 gas. (Figures S7, S8, and S9).

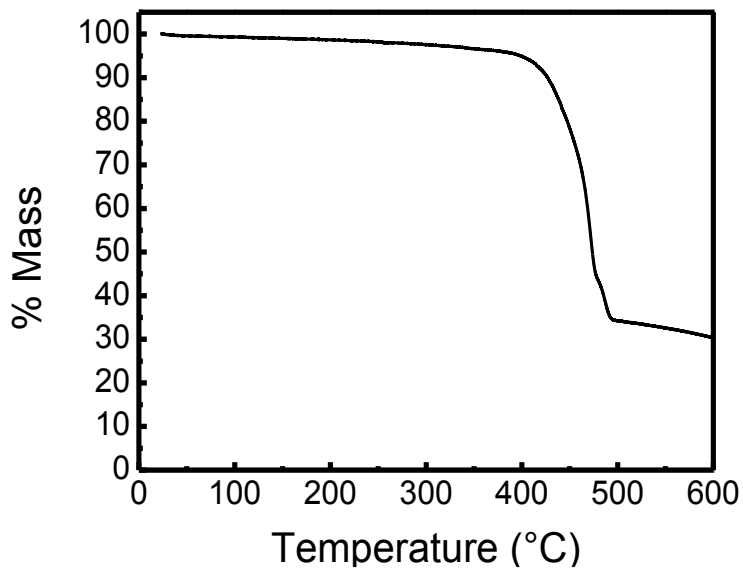


Figure S9. TGA trace of activated UMCM-10.

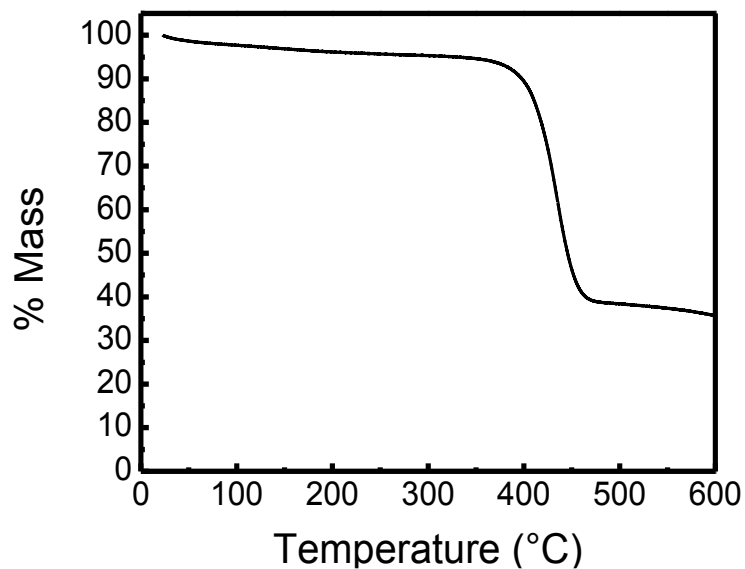


Figure S10. TGA trace of activated UMCM-11.

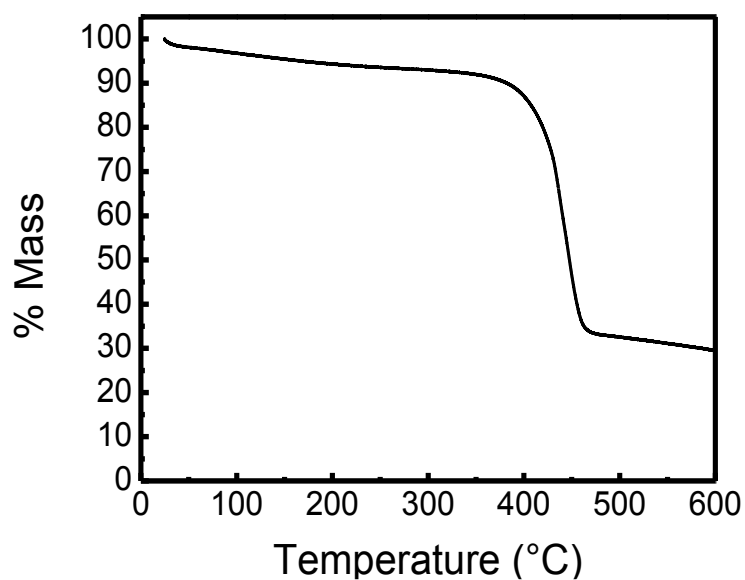


Figure S11. TGA trace of activated UMCM-12.

6. Gas sorption measurements of UMCM-4, -10, -11, -12

N₂ adsorption/ desorption isotherms were measured volumetrically at 77K in the range of $1.00 \times 10^{-5} \leq P/P_0 \leq 1.00$ with an Autosorb-1C outfitted with the micropore option by Quantachrome Instruments (Boyton Beach, Florida, U.S.A.) running version 1.2 ASwin software package. Ultra-high purity He (99.999%, for void volume determination) and N₂ (99.999%) were purchased from Cryogenic Gases and used as received.

Ar sorption experiments were performed in order to determine pore size distribution of materials (Figures S11-13) at 87K in the range of $1.00 \times 10^{-5} \leq P/P_0 \leq 1.00$. Ultra-high purity Ar (99.999%) was purchased from Cryogenic Gasses. Pore size distributions

were calculated applying Non-linear Density Functional Theory (NLDFT) zeolite/silica equilibrium transition kernel for Ar adsorption at 87K based on cylindrical pore model as implemented in version 1.2 of the ASWin software package.

H₂ and CO₂ adsorption/ desorption isotherms were measured volumetrically at 77K and 195 K respectively with an Autosorb-1C outfitted with the micropore option by Quantachrome Instruments (Boyton Beach, Florida, U.S.A.) running version 1.2 ASwin software package. Ultra-high purity H₂ (99.999%) and CO₂ (99.999%) were purchased from Cryogenic Gases and used as received.

Table 2. Predicted and experimental surface areas for activated materials obtained from N₂ isotherms

MCP	Predicted surface area (m ² /g) ⁶	Experimental BET surface area (m ² /g) determined from BET plots following self-consistency criterion ⁷
UMCM-4	3725	3632
UMCM-10	4475	4001
UMCM-11	4617	1525
UMCM-12	4756	4849

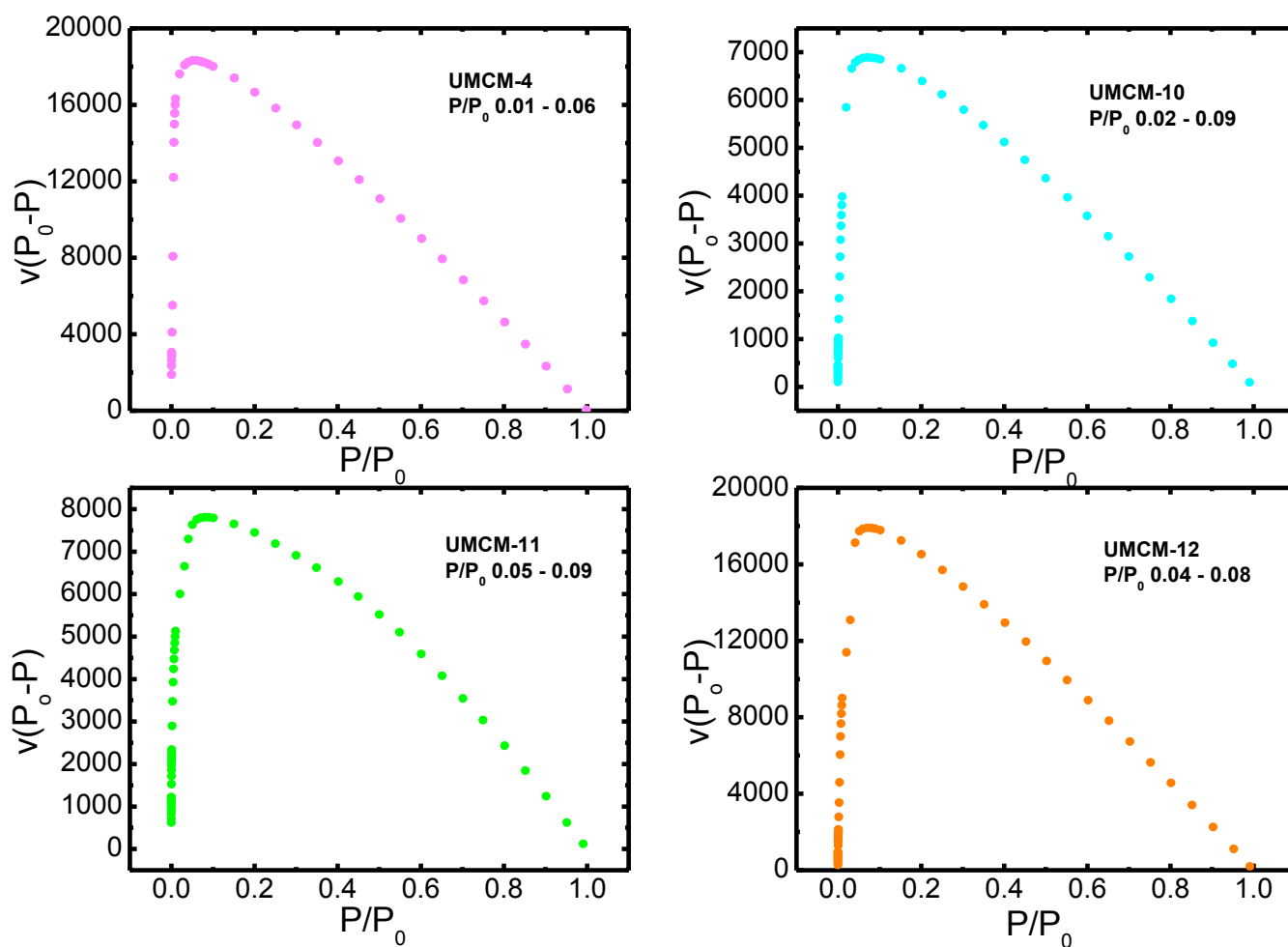


Figure S12. Self consistency plots for determining P/P_0 range for BET analysis based on isotherms shown in Figure 4.

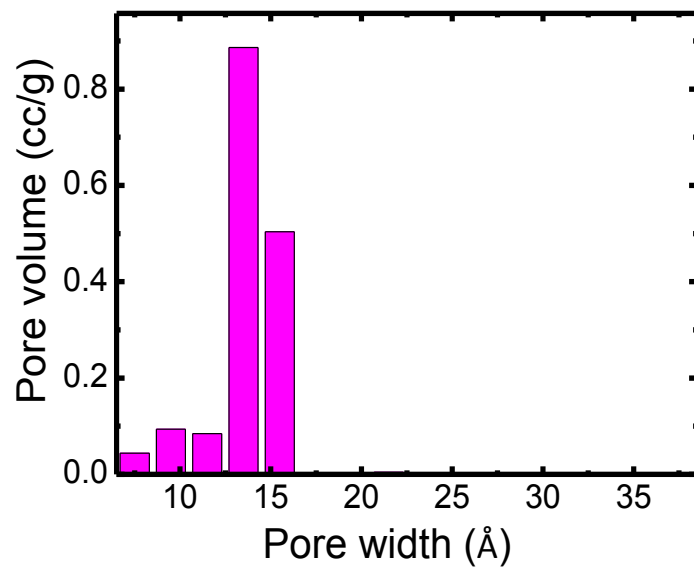


Figure S13. Pore size distribution of activated UCM-4.

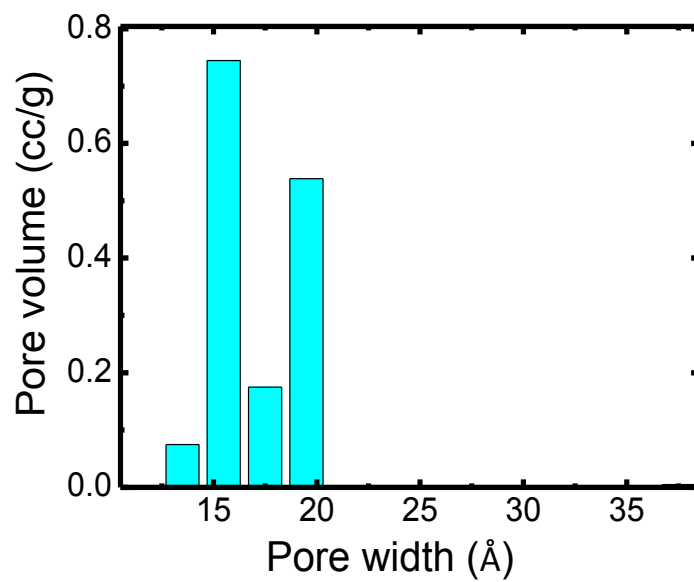


Figure S14. Pore size distribution of activated UCM-10.

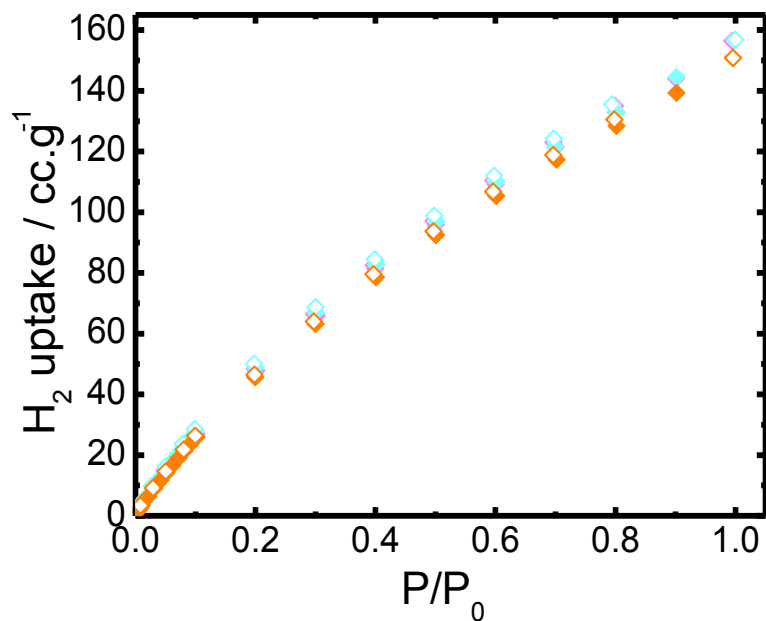


Figure S15: H₂ sorption isotherms of UCMCM-4 (purple), -12 (orange), and -10 (blue).

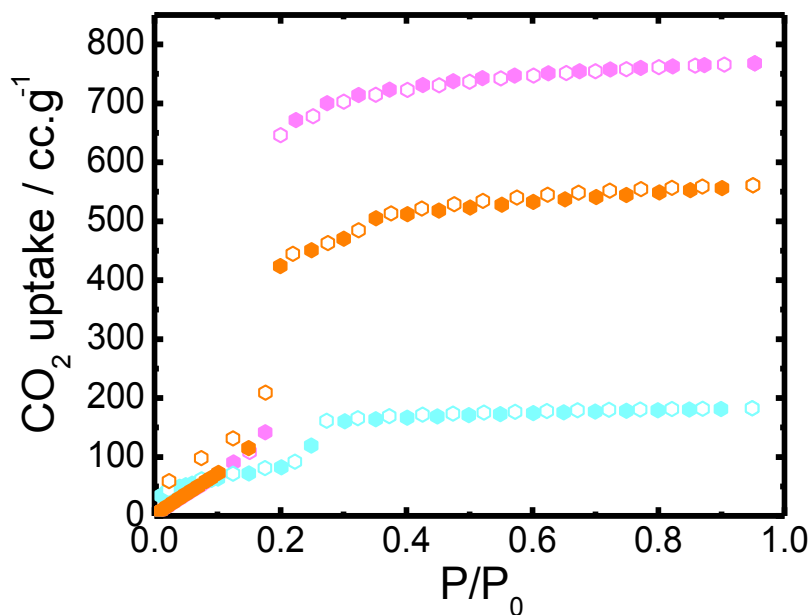


Figure S16: CO₂ sorption isotherms of UCMCM-4 (purple), -12 (orange), and -10 (blue).

7. PXRD patterns of UCMCM-4, -10, -12 at elevated temperatures and air

Variable temperature Powder X-ray diffraction data were collected on a Bruker D8 Advance Diffractometer having Bragg-Brentano geometry. The CuK α radiation source was operated at 40 V and 40 mA. Activated samples were ground and evenly dispersed on

a low background quartz plate placed on a hot stage. The diffraction patterns were collected at different temperatures under 1 sec/step scan rate.

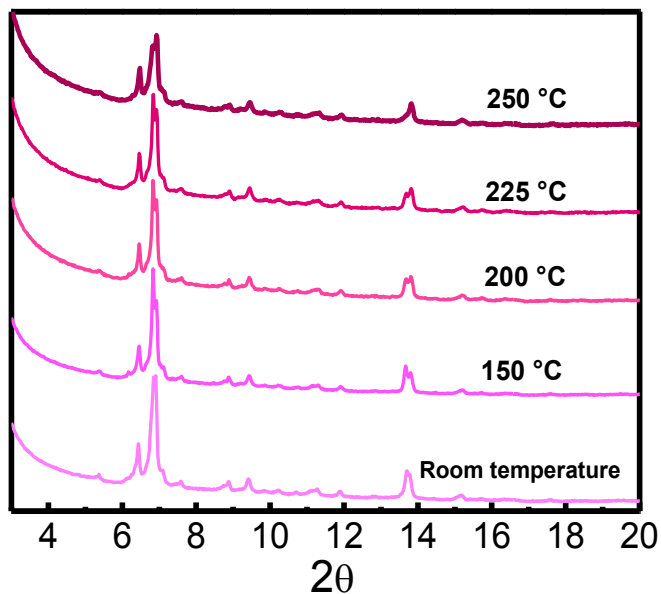


Figure S17. PXRD pattern of activated UMCM-4 at different temperatures.

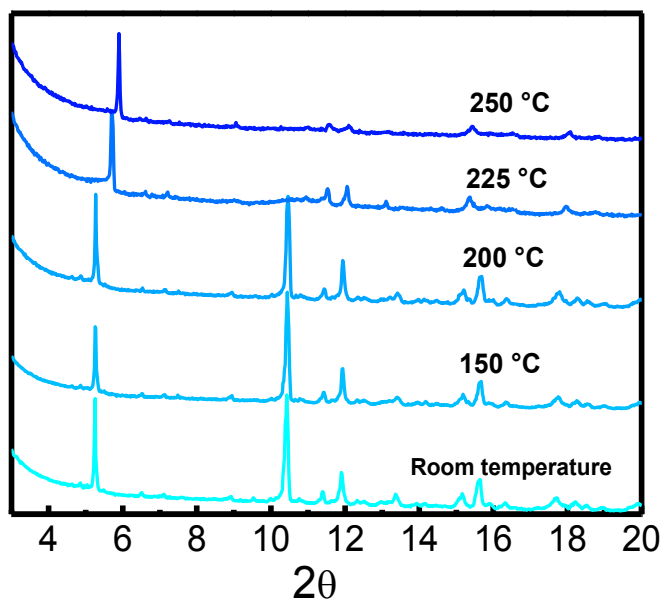


Figure S18. PXRD pattern of activated UMCM-10 at different temperatures.

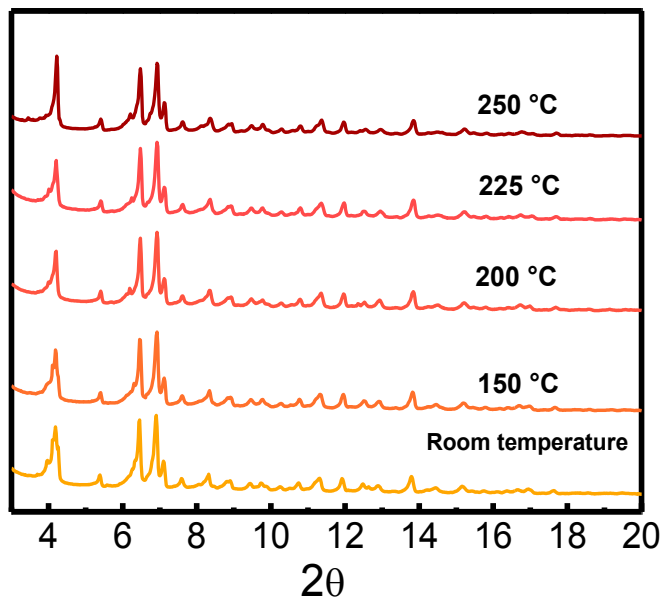


Figure S19. PXRD pattern of activated UCM-12 at different temperatures.

Samples after exposure to air for 12 hours were soaked in mineral oil before collection of powder X-ray diffraction data. Data were collected on Rigaku R-Axis Spider diffractometer with an image plate detector and $\text{CuK}\alpha$ radiation operating in transmission mode. The powder samples were rotated on the goniometer in ϕ and oscillated in ω to minimize preferred orientation.

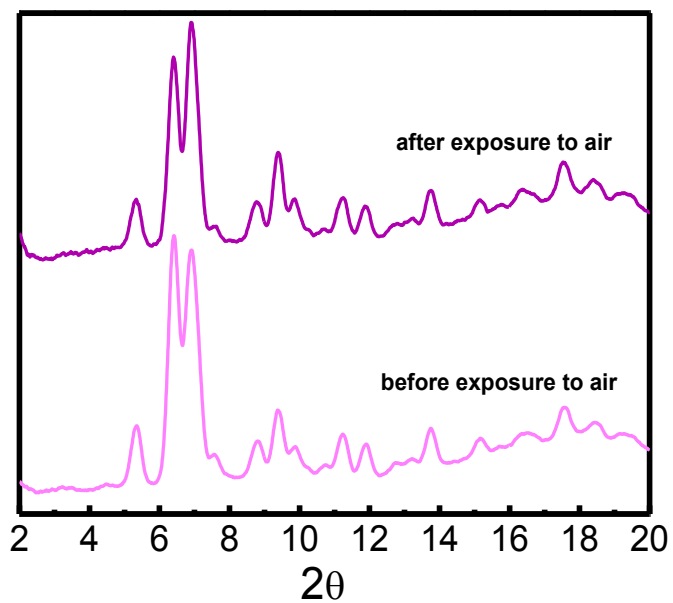


Figure S20. PXRD pattern of activated UCM-4 before and after exposure to air.

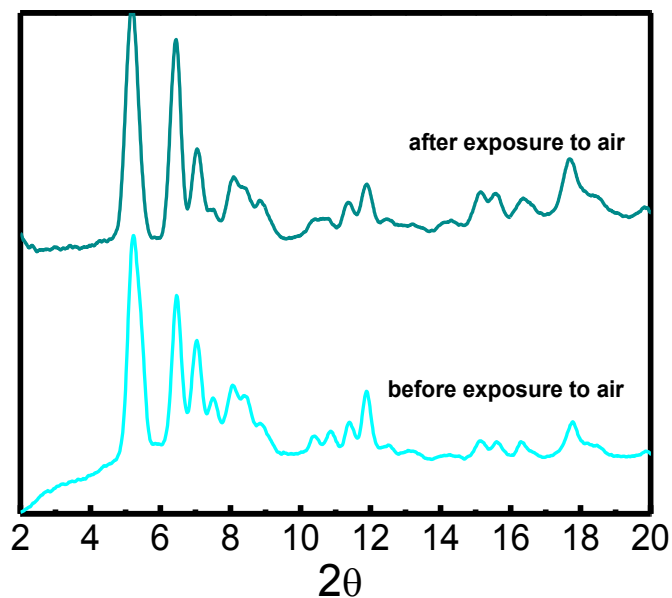


Figure S21. PXRD pattern of activated UCM-10 before and after exposure to air.

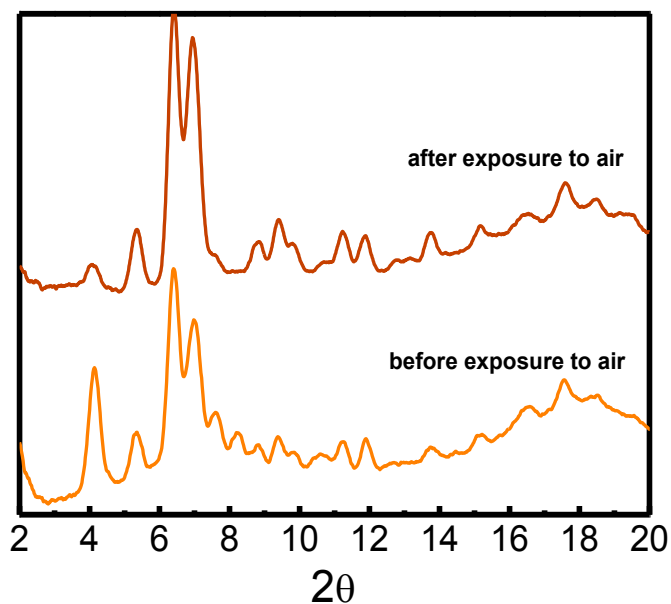


Figure S22. PXRD pattern of activated UCM-12 before and after exposure to air.

8. Microscopic images of dye diffusion experiments

MCP crystals were immersed in CH_2Cl_2 solution saturated with dye and containing additional solid dye solution at room temperature for 1 day and then washed with fresh CH_2Cl_2 5 times followed by immersion in mineral oil. Optical micrographs of crystals (Figures S14-16) after dye impregnation were taken with a Spot Flex camera fixed to a Leica DMLP microscope. All scale

bars indicate a distance of 100 μm . In each case, the crystals were sectioned to confirm that dye had penetrated to the centers of the crystals rather than outer surfaces.

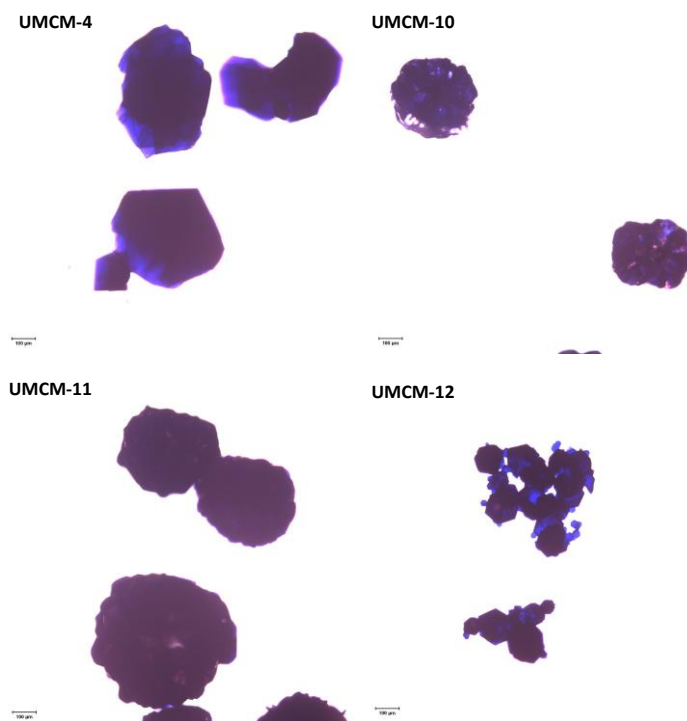


Figure S23. Microscopic images of dyed crystals of UMCM-4, -10, -11, -12 after Nile red dye diffusion.

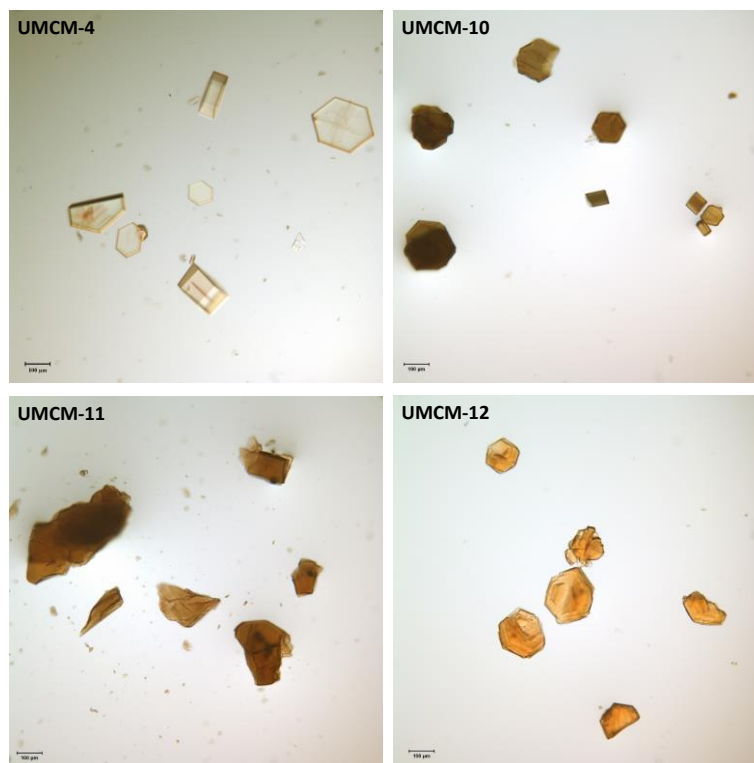


Figure S24. Microscopic images of dyed crystals of UMCM-4, -10, -11, -12 after Reichardt's dye diffusion.

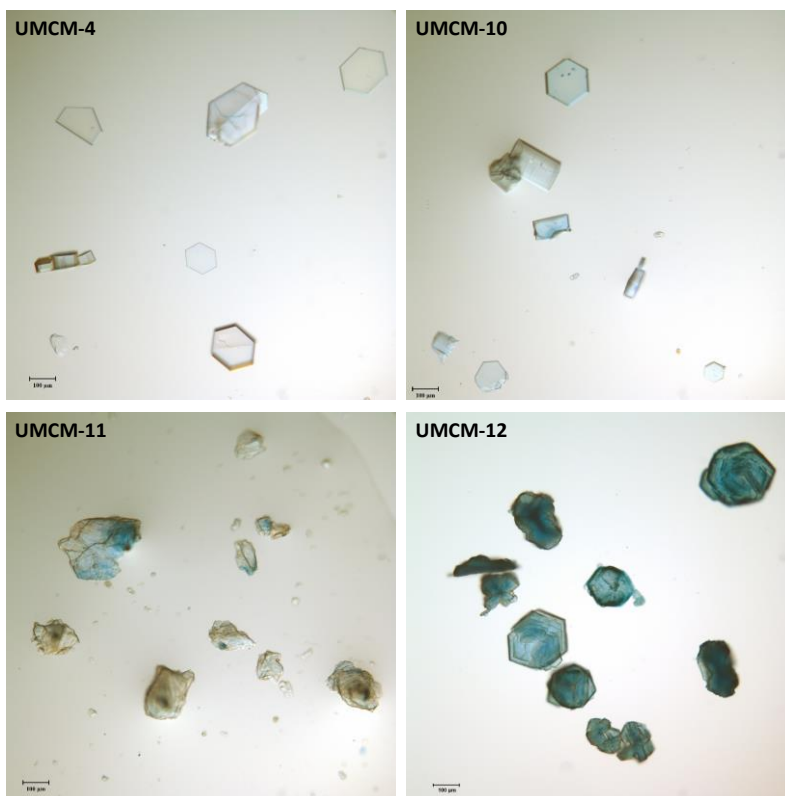


Figure S25. Microscopic images of dyed crystals of UMCM-4, -10, -11, -12 after Coomassie Brilliant Blue dye diffusion.

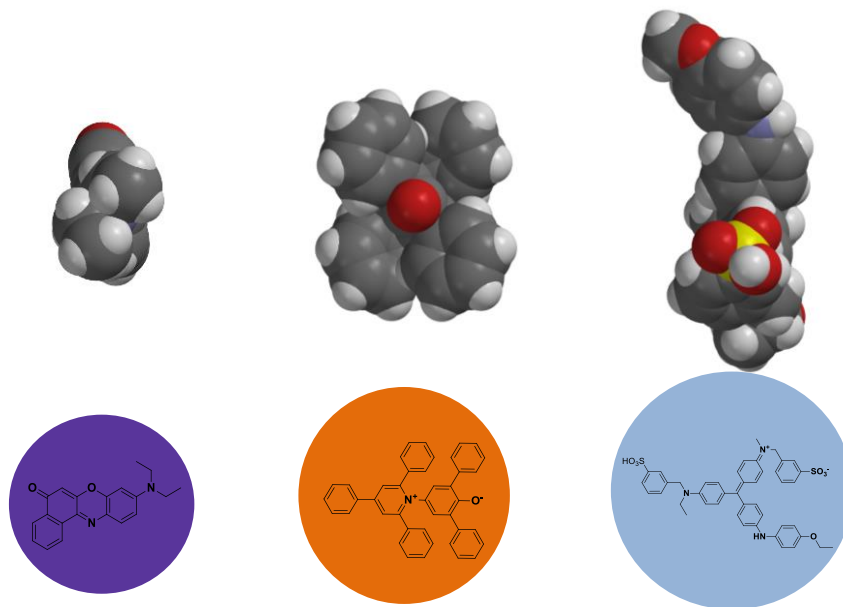


Figure S26. Kinetic diameters of dye molecules were approximated using the minimum cross-sectional area and taking van der Waals radii of atoms into account.

9. Linear dichroism experiment on UMCM-4 crystals

Optical micrographs of UMCM-4 crystals housing (Figures S18) after Nile Red dye diffusion were taken with a Spot Flex camera fixed to a Leica DMLP microscope. The systematic alignment of dye inside the pores of UMCM-4 causes different absorbance of light linearly polarized with different direction.

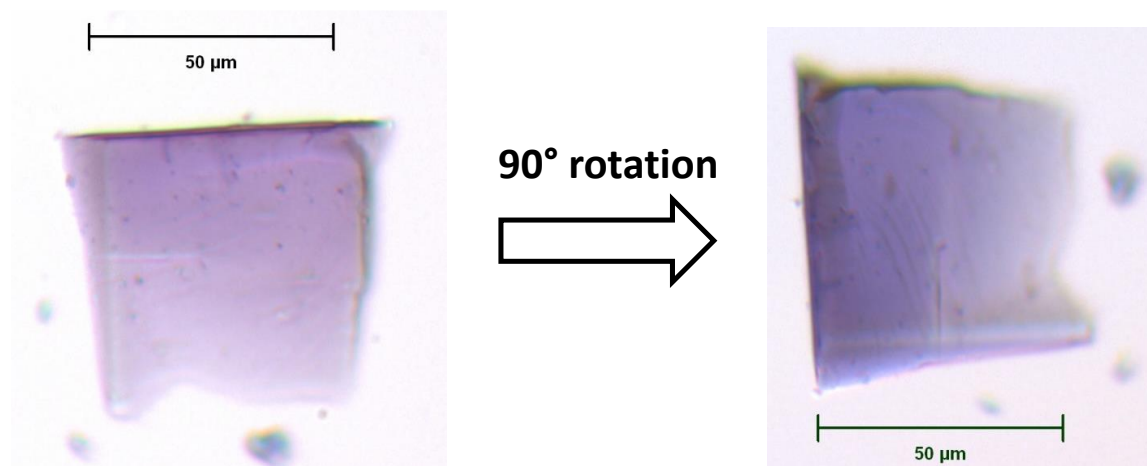


Figure S27. Microscopic images of UMCM-4 crystal housing oriented Nile Red dye molecules taken before and after 90° rotation with respect to plane polarized light. Exposure time was held constant.

References

1. T.-H. Park, K. Koh, A. G. Wong-Foy and A. J. Matzger, *Cryst. Growth Des.*, 2011, **11**, 2059-2063.
2. T. M. Fasina, J. C. Collings, J. M. Burke, A. S. Batsanov, R. M. Ward, D. Albesa-Jove, L. Porres, A. Beeby, J. A. K. Howard, A. J. Scott, W. Clegg, S. W. Watt, C. Viney and T. B. Marder, *J. Mater. Chem.*, 2005, **15**, 690-697.
3. H.-L. Jiang, D. Feng, T.-F. Liu, J.-R. Li and H.-C. Zhou, *J. Am. Chem. Soc.*, 2012, **134**, 14690-14693.
4. G. M. Sheldrick, *SHELXS '97 and SHELXL '97*. (University of Göttingen, Germany, 1997).
5. a) A. L. Spek, *J. Appl. Cryst.*, 2003, **36**, 7-13 ; b) A. L. Spek, *Acta Cryst. D65*, 2009, v. **51012**, 148-155.
6. T. Düren, F. Millange, G. Férey, K. S. Walton and R. Q. Snurr, *J. Phys. Chem. C*, 2007, **111**, 15350-15356.
7. J. Rouquerol, P. Llewellyn and F. Rouquerol, *Studies in Surface Science and Catalysis*, 2007, **160**, 49-56 (Eds.: F. R.-R. J. R. P.L. Llewellyn, N. Seaton), Elsevier.